The structure of the cytochrome P450cam-putidaredoxin complex determined by paramagnetic NMR spectroscopy and crystallography

Hiruma, Y.

CHAPTER 1

General introduction

P450 discovery and history

It was in 1954 in Philadelphia that Klingenberg discovered a novel carbon monoxide-binding pigment in rat liver microsomes.[1] He added a trace of sodium dithionite and bubbled carbon monoxide while studying the kinetics of cytochrome b_5 in rat liver. Unexpectedly, he observed the appearance of a prominent absorption peak at 450 nm. This unique optical spectral change in the presence of carbon monoxide shared no resemblances with any other known metallo-proteins. In 1962, Omura repeated Klingenberg's experiments and named the mysterious "microsomal carbon monoxide-binding pigment" cytochrome P-450. "P" is the abbreviation of pigment and "450" was named after the unique optical absorption peak at 450 nm. In the first paper of "cytochrome P450", Omura reported that the carbon monoxide-binding pigment in liver microsomes was a novel hemoprotein. The molar extinction coefficient of characteristic 450 nm peak (ε_{450nm} = 91 $mM^{-1}cm^{-1}$) described in the paper is still widely used today to quantify the P450 content in biological samples.[1]

P450 research soon expanded into various fields, from physiological functions to industrial chemistry. In the year following the first P450 paper, Estabrook, Cooper and Rosenthal reported that cytochrome P450 was involved in the biosynthesis of steroid hormones in bovine adrenal glands.[2] They also found that P450 is an enzyme that catalyzes hydroxylation reactions of substrates using molecular oxygen. In 1965, P450 in rat liver microsomes was shown to participate in the oxidative metabolism of pharmaceutical compounds.[3] At the end of 1960's, the presence of P450 was discovered in various tissues and organisms.[4] Today, at least 57 different P450 genes are known in human beings;[5] some of which are involved in the metabolism of sex hormones and others in the biosynthesis of cholesterol. Besides the unique absorption peak at 450 nm, P450 members share conserved amino acid sequences and a similar fold. In 1987, Nebert *et al.* coined the nomenclature of "CYP" to classify various P450 into families and sub-families based on primary sequences.[6] The family tree generated by CYP classification indicated that all of the P450 in various organisms evolved from a single ancestral P450. Thus, P450 members are all part of the CYP superfamily.[1]

Practical applications of P450

Nowadays, approximately two thousand papers on CYPs are published annually.[1] One of the most useful features of P450 is regio- and stereo-specific hydroxylation. For instance, while chemical synthesis of drugs derived from vitamin D_3 requires 20 steps with low yield, P450 (CYP107) dependent conversion proceeds through a single step.[4] At present several millions of patients are prescribed steroidal medicines, including cortisol and low density lipoprotein (LDL)-cholesterol lowering drugs. In 1952, a microbiologist called Murray published the first report of cortisol production in a single step by the use of the fungus *Curvulavria lunata*.[7] The mycelium of this fungal species was later discovered to possess P450lun, which converts 11-deoxycortisol to

cortisol.[8] Even to date, industrial production of cortisol depends on the immobilized *C. lunata* and overexpression of P450lun is attempted to increase the product yield.[4] The invention of the "blue rose" is one of the most stunning applications of P450. Over the centuries, the creation of blue roses had been believed to be impossible due to the limitation of available colors of roses.[4] However, in 2007, an industrial team in Japan has made the blue rose possible by introducing P450 gene (CYP75A) from viola (Figure 1).[9]

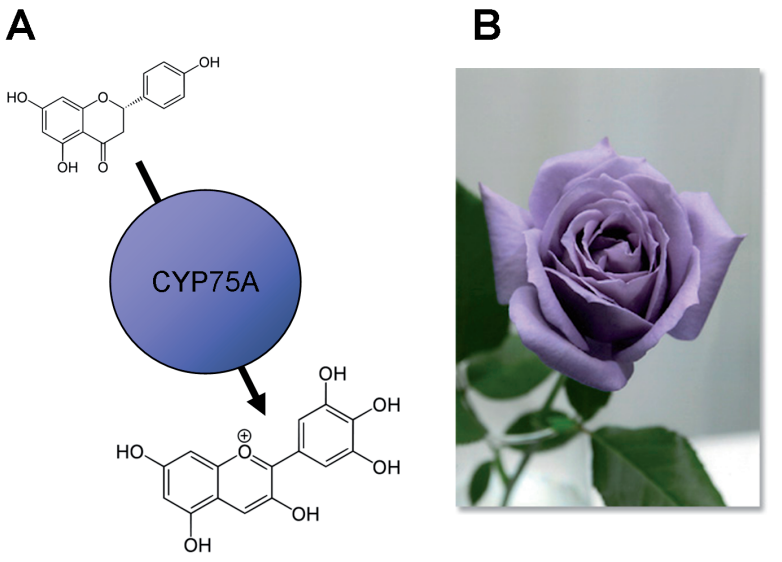

Figure 1. Production of blue roses by CYP75A. (A) CYP75A catalyzes the hydroxylation of flavanone to generate blue pigment, delphinidin. (B) Blue rose created by a Japanese company, Suntory. The picture was taken from www.suntory.com.

P450cam history

For over a decade after the initial discovery of rat liver microsomal P450, CYPs were believed to be present only in higher eukaryotes.[1] However, in 1968, Katagiri *et al.* reported that an NADH-dependent P450 system was found in *Pseudomonas putida*.[10] This bacterial P450 system consists of three soluble components, namely, an FAD-containing flavoprotein, an iron-sulfur containing ferredoxin and P450. Electrons are relayed from NADH to P450 to catalyze the hydroxylation of D-camphor. Due to its unique physiological substrate, *P. putida* P450 has been commonly known as P450cam. Moreover, the water solubility of P450cam advanced the P450 research and P450cam has become a model system of mammalian P450.[1] In 1985, Poulos reported the first crystal structure of P450cam, which illustrates the unique coordination of a thiolate to a heme iron.[11] The biophysical and biochemical analysis expanded and P450cam

has become the most extensively characterized P450 family member. By 2013, 109 different structures of P450cam had been deposited in protein data bank.

P450cam catalytic cycle

Hydroxylation of camphor is part of a metabolic process in *Pseudomonas putida* to harvest carbon and obtain energy. Utilizing an oxygen molecule, P450cam catalyzes regio- and stereo-specific hydroxylation of D-camphor and generates 5-*exo*-hydroxycamphor.[10] As shown in Figure 2, the enzymatic activity of P450cam proceeds through the series of the catalytic events: i) substrate binding; ii) the first electron transfer (ET1); iii) oxygen binding; iv) the second electron transfer (ET2); v) proton transfer; vi) oxygen activation and hydroxylation reaction; vii) product release.

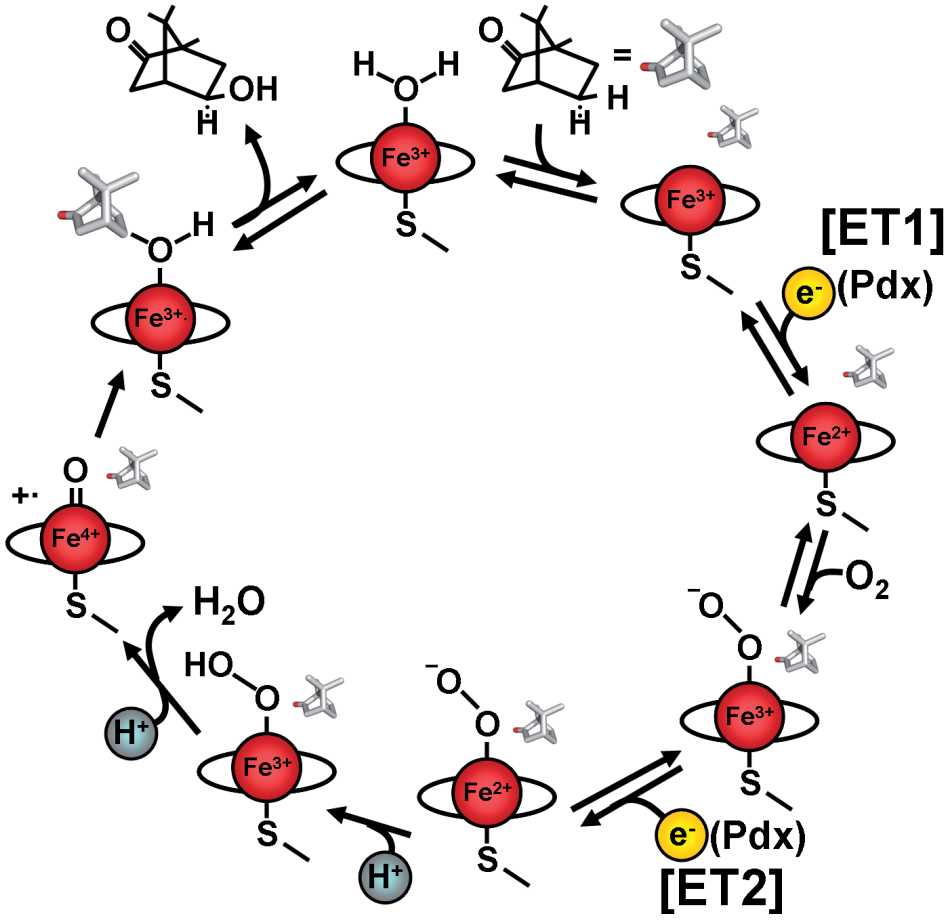

Figure 2. Catalytic cycle of P450cam.[12]

In the resting state of P450cam, the heme iron is coordinated by a water molecule as the sixth ligand. The substrate-free form of P450cam has been shown to exhibit an "open" conformation to allow the substrate to access to the active site.[13] The reaction cycle is initiated by binding of substrate, camphor. Camphor binding changes the spin state of heme iron from low spin to high spin. It was well documented that the transition of spin state is accompanied by the change of redox potential.[1] In the resting state, the substrate-free form of P450cam exhibits a redox potential of –300 mV.[14] However, upon binding of camphor, redox potential is elevated to –170 mV,[14] which promotes the first ET event.[1] The ferric state (Fe^{3+}) of P450cam accepts the first electron from the physiological ET partner protein, putidaredoxin (Pdx). Recent results of mutagenesis and kinetics studies suggested that this ET event is the rate-limiting step for catalytic turnover (41 s^{-1}).[15] Upon binding of an oxygen molecule, the ferrous heme iron (Fe^{2+}) binds O_2 to form oxygenated P450cam.[12] In the second ET event, Pdx has two roles; ET and effector activity. The binding of Pdx to oxygenated P450cam results in some structural change in the P450cam. This conformation shift facilitates the ET2 as well as enables the following events of the oxygen activation and product formation.[16] The underlining mechanism of the Pdx effector activity is still under debate. However, the stringent requirement of Pdx for the ET2 process indicates that there is a drastic difference between ET1 and ET2.[15] The second electron is delivered to the ferrous iron and activates the O-O bond. After the protonation of the activated oxygen molecule, the oxenoid-iron (Fe^{4+}=O), also known as compound I, is formed by displacement of a water molecule. The oxenoid-iron reacts with the camphor molecule to produce 5-*exo*-hydroxycamphor. The dissociation of the product from active site is accompanied by repositioning a water molecule as the axial ligand of the heme iron and reaction cycle in complete.[12]

P450cam structural properties

P450cam consists of 414 amino acid residues with a molecular weight of 46.6 kDa. As an archetypical P450 enzyme, its type b heme iron is coordinated by an axial thiolate ligand of Cys357 (Figure 3).[17]

The secondary structure elements of P450cam comprise thirteen α-helices and five β-sheets. The nomenclatures of the A–L helices and β1–5 sheets are based on their order in the P450cam amino acid sequence (Figure 4). The B' helix has been added to the system by Poulos and co-workers after they found the additional α-helix in high-resolution crystal structure.[19] The proximal and distal sides of P450cam have distinct functions. It has been reported that Pdx binds to the proximal side of P450cam while the distal side allows substrate access to the active site.

The unique appearance of the Soret band at 450 nm is attributed to the reduction of the heme iron and the concomitant binding of carbon monoxide.[12] Besides CO and camphor, P450cam can accommodate a variety of compounds in the substrate

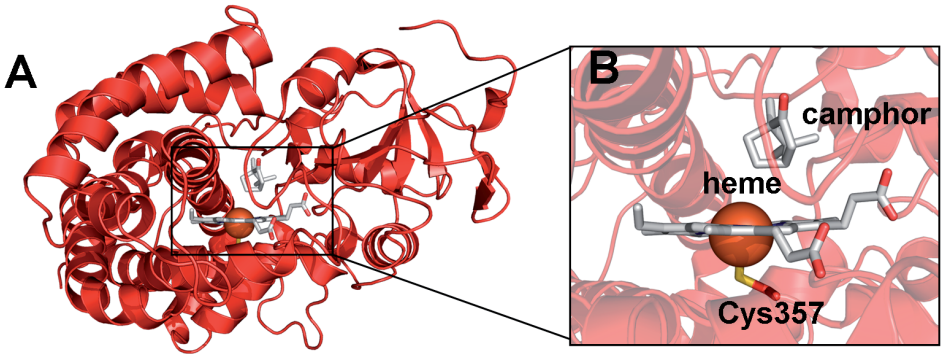

Figure 3. Crystal structure of P450cam bound to camphor (PDB entry, 1DZ4[17]). (A) ribbon representation of P450cam. (B) Zoom in view of active site of P450cam. The brown sphere represents the heme iron.

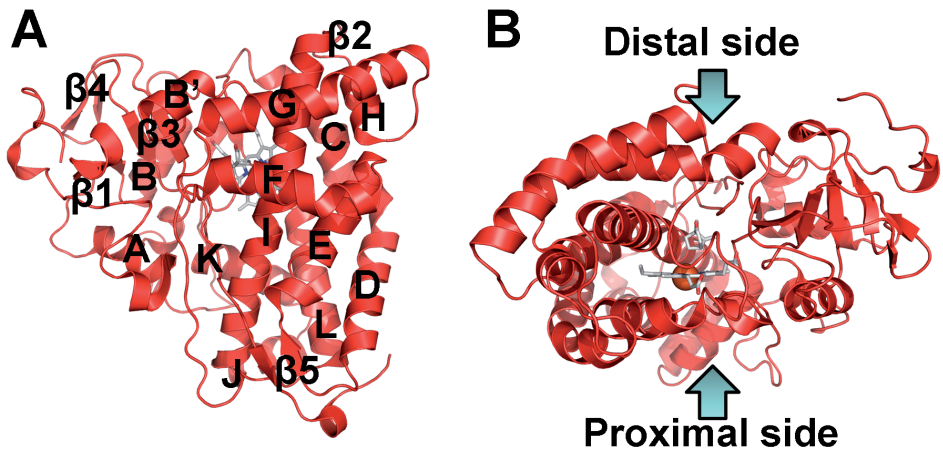

Figure 4. Ribbon representation of P450cam structures (PDB entry 1DZ4[17]). (A) Nomenclature of the secondary structure elements of P450cam, facing the distal side (B) Arrows indicate the proximal and distal sides of the protein.

binding site. For instance, P450cam binds small molecules such as cyanide, imidazole, cysteine, DTT as well as substrate analogues such as adamantane-derivatives.[12] The binding of these molecules influences the coordination sphere of the iron, which can result in transitions of the spin state of ferric iron between high and low.[12] Although a number of ligands were known to interact with P450cam, the process of substrate binding had puzzled researchers for decades because atomic resolution structures of P450cam show that there is no channel present on the protein surface to allow a substrate to access the active site. In 2001, Dunn *et al.* demonstrated the opening of

substrate access channel of P450cam by crystallizing P450cam bound to ruthenium sensitizer-linked substrates (Figure 5).[18] The adamantane moiety of the complex binds to the active site of P450cam and its ruthenium tethered linker protrudes toward the protein surface, thereby forcing the access channel to be in the open conformation. In 2010, Lee *et al*. solved the crystal structure of substrate-free form, which showed the location of the access channel beyond any doubts.[13]

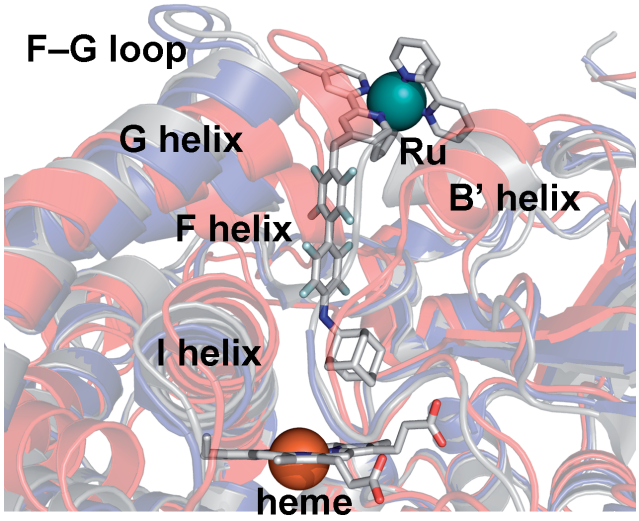

Figure 5. Cartoon representation of the overlaid P450cam structures. Red, gray and blue represent P450cam bound to camphor (PDB entry 1DZ4[17]), ruthenium complex (1K2O[18]) and substrate-free (3L61[13]), respectively. The sticks chelating to the green sphere illustrate ruthenium sensitizer-linked substrate.

The helices B', F, G and I as well as the F–G loop have been found to be involved in the conformation change between the open and closed state of the substrate access channel.[13, 18] It has been speculated that the synergistic movement of the B', F and G helices optimizes the efficiency of the substrate uptake as well as the catalytic reaction.[13] The potassium ion binding site is another key feature of B' helix.[19] It has been reported that the binding affinity of the substrate is dependent of the concentration of potassium ions. At a high concentration of potassium (> 50 mM), the stability of closed conformation increases, thereby decreasing the dissociation rate of the substrate.[20, 21] Mutagenesis demonstrated that the I helix residues, Asp251 and Thr252, facilitate the proton transfer to the activated oxygen molecule in the active site.[22] To further investigate the structure dynamics and the catalytic mechanism of P450cam, Pochapsky and co-workers studied the P450cam structure in solution state by NMR spectroscopy.[23, 24] Their NMR results indicated that the active site of P450cam

is more mobile than previously described.[24] In particular, significant dynamics was observed for the B' helix.[23] It was speculated that the plasticity of the active site contributes to the ability of P450cam to accommodate a wide variety of substrates as well as inhibitors.

Putidaredoxin

Putidaredoxin (Pdx), a [2Fe-2S] cluster containing ferredoxin, acts as a physiological electron transfer partner of P450cam in *Pseudomonas putida*. It shuttles two electrons from putidaredoxin reductase to P450cam during the camphor hydroxylation reaction.[25]

The redox center of Pdx consists of two iron atoms (Fe1 and Fe2), both of which are coordinated to the two sulfide ions as well as two thiol groups of the cysteine residues. Atom Fe1 is positioned in close proximity of the protein surface (Figure 6). Therefore, it is believed to play a major role in the electron transfer process.

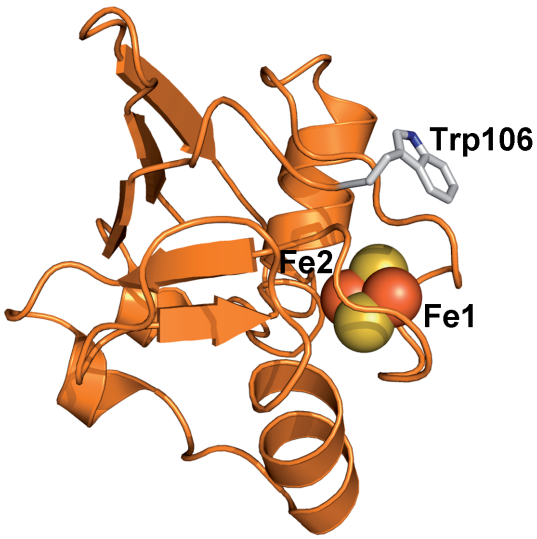

Figure 6. Ribbon representation of Pdx (PDB entry, 1XLP[26]). Sticks and spheres illustrate the side chain of Trp106 and [2Fe-2S] cluster, respectively.

Over the decades, the [2Fe-2S] cluster of Pdx had hindered the structural studies of the protein. In NMR studies, vital information about the active site of the protein cannot be determined due to the significant broadening effect caused by high-spin state of iron atoms. Pochapsky and co-workers challenged the problem by replacing two irons by gallium ions.[27] However, the substitution of the redox center leads to a structure change in Pdx. The crystallization of Pdx was also very challenging. At high concentrations of the protein, the progressive loss of the iron sulfur cluster from the

protein was observed. The identification of surface exposed cysteine residues led to a breakthrough in Pdx crystallization. Pdx contains six endogenous cysteine residues, four of which are the ligands for the two irons. It was found that the substitution of Cys73 and Cys85 greatly enhances the stability of the iron sulfur cluster.[28] In 2003, Sevrioukova *et al.* solved the crystal structures of Pdx C73S and Pdx C73S/C85S variants.[28] With the exception of the residues in the active site, the structures obtained by X-ray crystallography and NMR were in good agreement. The structural analysis indicated that the oxidized state of Pdx exhibits more dynamic than the reduced state.[26, 29] The regions nearby the [2Fe-2S] cluster (Tyr33, Asp34, His49 and Tyr51) as well as the C-terminus (Val74–Asn82 and Pro102–Trp106), in particular, were found to be mobile in the oxidized Pdx.[29] These residues play key roles in the recognition of the partners PdR and P450cam.

Pdx comprises of 106 amino acid residues of which single tryptophan is present at the C-terminus. Despite the hydrophobic nature of the side chain, Trp106 of Pdx is fully exposed on protein surface and exhibits rotational freedom on the timescale of nanoseconds to sub-nanoseconds.[29] Early mutagenesis studies demonstrated that Trp106 primarily functions as a recognition motif for the partners.[30] The binding affinity and electron transfer rates dramatically reduced when Trp106 is either substituted or deleted from Pdx WT.[15, 30] The most intriguing feature of Pdx function is the effector activity, in which Pdx binding induces a conformation change in P450cam to start the catalytic action of the camphor hydroxylation reaction.[25] However, the underlying mechanism of the effector activity is poorly understood. Currently, two contradictory mechanisms have been proposed. According to Pochapsky and co-workers, Pdx acts as an effector by inducing a conformation change in oxy-P450cam.[31] A structural change in the Pdx binding site mechanically transmits to remote regions of P450cam. The isomerization of Ile88–Pro89 amide bond has been reported to be the key feature of the conformation change.[32] According to this study Pdx binding converts the *trans* conformer of the peptide bond into the *cis* conformer, which leads to the reorientation of the substrate in the active site as well as the closure of the substrate access channel. The substrate is thereby trapped in the active site of P450cam, which minimizes the solvation of the substrate and the escape of harmful peroxide intermediates.[31, 33]

The recently determined crystal structure of Pdx-bound P450cam exhibits the open configuration and the substrate and/or product can freely access to the active site (structure details are discussed in the Chapter 3). Based on this observation, Poulos and co-workers proposed that the effector role of Pdx is to cause P450cam to open up the substrate access channel.[34] Opening of the substrate access channel allows the catalytic water molecule to enter the active site. It was speculated that this water mediates the hydrogen bonded networks required for the proton transfer.[34] Another key residue, Asp251, is freed from the salt bridge during the conformational shift to the open state. Together with the adjacent residue, Thr252, Asp251 plays a vital role in the proton transfer for O–O bond heterolysis.[34] The opening is thought also to

cause a change in the iron spin state and such a spin state shift has been observed in a resonance Raman spectroscopy study.[35] Champion and co-workers reported that Pdx binding produces a low spin state of heme iron, reflecting the open conformation of P450cam.[35] A recent study using double electron-electron resonance (DEER) spectroscopy indicated that the conformation change of P450cam is dependent on the oxidation states of Pdx.[21] In line with the suggestions of the previous studies, the authors report that binding of oxidized state of Pdx induces P450cam to be in open conformation. However, reduced and CO-bound P450cam remains in the closed conformation in the complex with the reduced state of Pdx.[21] Thus, not all studies paint a consistent picture of the mechanism of the effector function of Pdx binding. This phenomenon remains to be elucidated.

Putidaredoxin reductase

Putidaredoxin reductase (PdR) is an FAD-containing flavoprotein (Figure 7). To reduce an oxygen molecule, P450cam requires two electrons. PdR transfers two electrons from NADH to Pdx which in turn shuttles them to P450cam. PdR consists of 421 amino acid residues and possesses FAD and NAD binding domains.[25]

The interaction of PdR with Pdx is often compared with the complex formation of adrenodoxin reductase (AdR) and adrenodoxin (Adx), which are the homologue of

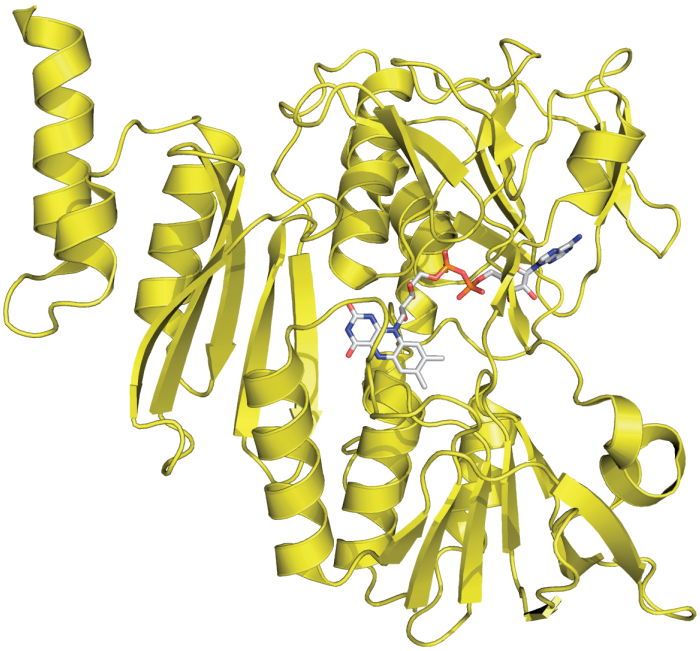

Figure 7. Ribbon representation of PdR (PDB entry, 1Q1R[36]). FAD is shown in sticks.

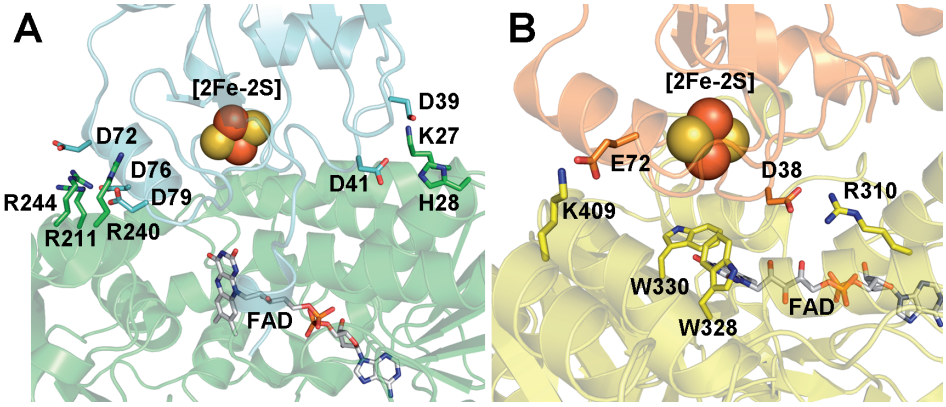

Figure 8. Cartoon representation of AdR-Adx and PdR-Pdx complexes. Sticks represent the side chains of the interaction residues and FAD. (A) Green and light blue represent AdR and Adx, respectively (PDB entry 1E6E[37]). (B) Yellow and orange represent PdR and Pdx, respectively (PDB entry 1Q1R[36]).

human proteins. The crystal structures of PdR-Pdx and AdR-Adx complexes highlighted the difference of binding modes in two systems (Figure 8).[25] The interaction of AdR-Adx complex is primarily driven by electrostatic interactions. The acidic patches on the Adx surface interact with the basic concave FAD-binding site of AdR.

PdR-Pdx binding, on the other hand, primarily involves hydrophobic contacts and polar interactions. Trp328 and Trp330 of PdR are key components of the complex formation and part of the electron transfer pathway between PdR and Pdx. The experimentally obtained ET rate from PdR to Pdx is 235 s^{-1} while theoretical maximal ET rate is estimated to be 2.7×10^5 s^{-1}. The difference of three orders of magnitude has been attributed to the reorganization energy of Pdx reduction.[25]

Protein-protein interactions

During protein complex formation, the proteins undergo at least are intermediate step (illustrated in Figure 9).[38] First, the proteins form an encounter complex in which one protein searches for the docking surface of the other and then the well-defined, final complex is formed. It has been speculated that the long-range electrostatic interaction drive the transient state of protein-protein interaction.[39-41] However, the recent results of paramagnetic NMR analysis suggested that hydrophobic interactions also play an important role.[42, 43] The primary role of the encounter state is to minimize the dimensionality search of optimal binding, and thus to enhance the number of productive collisions. In classic textbooks, the dynamic encounter state is assumed to exist only transiently and to rapidly form the final well-defined complex. However, the latest NMR spectroscopy data have indicated that the encounter complex represents a significant population in weak protein-protein complexes (e.g. electron transfer

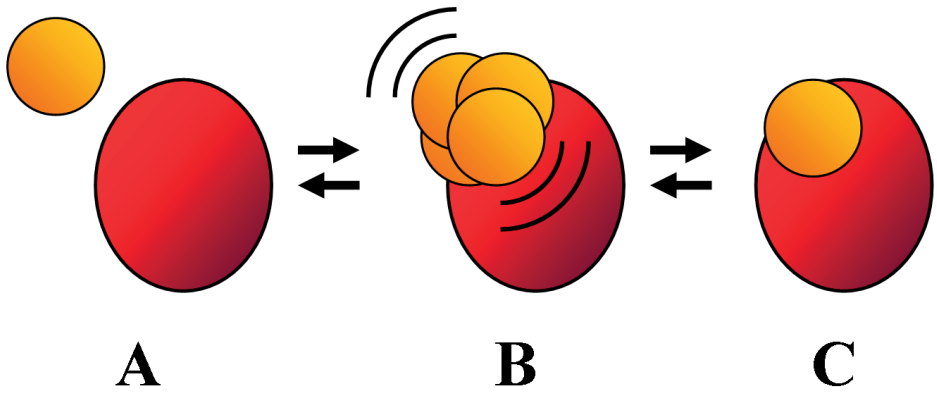

Figure 9. Model of transient protein complex formation. A) Two proteins come close together by diffusion. B) The encounter complex: proteins sample each other's surface in multiple orientations. C) A single, well-defined complex is formed.

protein complexes).[38, 44] Kinetic data analysis also suggested that some proteins achieve electron-transfer active states in the encounter complex rather than in a single well-defined complex.[39, 40, 45-48]

Paramagnetic NMR probes

A variety of paramagnetic NMR techniques have been rapidly developed in the last few decades. They enable protein chemists to analyze not only structural information of protein interfaces but also kinetics, binding affinity and transient intermediates of protein interactions.[49, 50] The presence of unpaired electrons causes paramagnetic effects in NMR spectra, which includes "line broadening" and "line shifts". Line broadening is the consequence of enhanced relaxation by unpaired electrons. Since the effect is proportional to the sixth power of distance between the electrons and observed nuclei, it has been used as a sensitive tool of distance measurement in proteins.[51] Line shifts in NMR spectra can be categorized as contact shifts and pseudocontact shifts. Contact shifts are caused by the delocalization of unpaired electrons onto observed nuclei and can be observed only upto several bonds away from the paramagnetic center. Pseudocontact shifts (PCS) result from dipolar interactions between the electron(s) and nuclei. The magnitude of a pseudocontact shift depends on the anisotropy of the magnetic susceptibility described by the $\Delta\chi$ tensors and is proportional to the third power of the distance between electron and nucleus.[51] Strongly paramagnetic metal ions can possess a large $\Delta\chi$ tensor, enabling the observation of pseudocontact shifts for nuclei far from the unpaired electron.[52] Pseudocontact shifts, thereby, provide restrains to refine structures of macromolecules.[50]

Lanthanoid ions (Ln^{3+}) are known to be excellent paramagnetic groups that possess unpaired electrons in the 4f orbitals. Different lanthanoids share similar ionic radii and geometries but exhibit a broad range of magnitudes of paramagnetic effects. For instance, lanthanum (La^{3+}) and lutetium (Lu^{3+}) ions are diamagnetic whereas dysprosium (Dy^{3+}), thulium (Tm^{3+}) and ytterbium (Yb^{3+}) ions are strongly paramagnetic.[52, 53] Therefore, lanthanoid ions are widely used for paramagnetic NMR studies.

The lanthanoid tags offer several distinctive advantages over conventional bivalent ion (Mn^{2+}, Co^{2+} etc.) probes. First of all, the substitution of different lanthanoid ions allows for a wide range of paramagnetic effects, providing a number of $\Delta\chi$ tensor values with the same probe. Secondly, some lanthanoids possessing a high anisotropy magnetic tensor are able to align slightly to the external magnetic field. Therefore, those lanthanoid-labeled proteins and protein complexes achieve partial molecular alignments in the absence of alignment media. Residual dipolar couplings can be therefore measured under the same conditions between unaligned sample and partially aligned sample. Since the alignment induced by a paramagnetic ion will not be limited by molecular size, lanthanoid tags are an attractive tool for RDC measurements in macromolecules as well as in the study of intermolecular interactions.[54]

Many kinds of lanthanoid tags have been published over recent years, including protein fusions with lanthanoid-binding peptides[55, 56] as well as lanthanoid-binding peptide that are attached via a disulfide bond.[57] Caged lanthanoid NMR probe version 7, CLaNP-7, is a synthetic lanthanoid chelating molecule developed for the

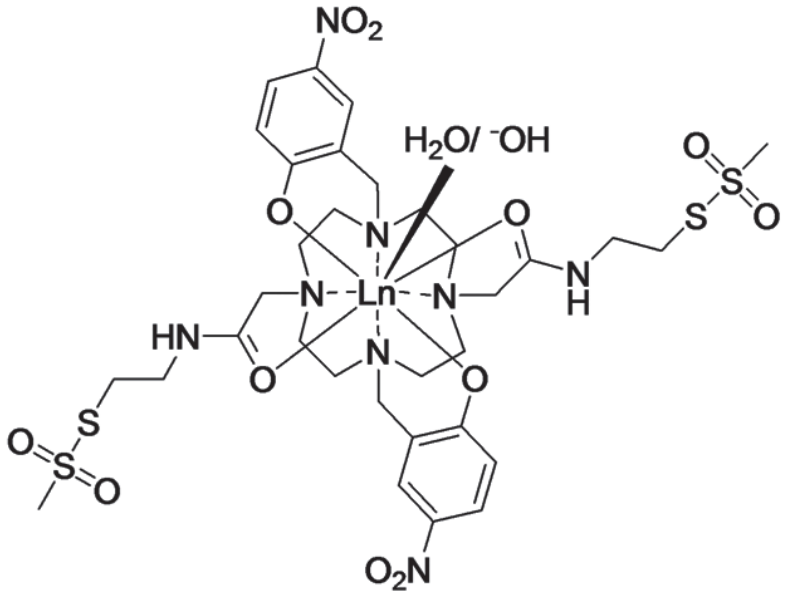

Figure 10. Caged lanthanoid NMR probe version 7, CLaNP-7.

attachment of lanthanoid atoms on protein surfaces (Figure 10).[58] It has been designed to fulfill the following criteria: i) the probe is capable of accommodating different lanthanoid atoms, allowing to observe a range of paramagnetic effects; ii) two thiol "arms" of the probe covalently binds to two cysteine residues on a protein surface. The "two-point attachment" restricts the flexibility of the probe movement, preventing averaging effects. The resonance averaging effect becomes detrimental when the magnitudes of the paramagnetic effects are strongly dependent on the distance between paramagnetic center and observed nuclei. It also reduces the degree of residual dipolar coupling (RDC) when the probe is used to induce partial alignment in a magnetic field.[59] With Tm^{3+} as a paramagnetic ion, CLaNP-7 showed PCS for nuclei as far as 60 Å distance from the lanthanoid. Tm^{3+} loaded CLaNP-7 induces RDC of about 20 Hz at 14 T (600 MHz) magnetic field strength.[58] Furthermore, paramagnetic relaxation enhancement caused by the gadolinium ion (Gd^{3+}) contained in CLaNP-7 is also a useful tool for macromolecular structure determination, with distances up to 45 Å measured accurately (Chapter 3).[60]

Pseudocontact shift

Pseudocontact shifts (PCSs) provide long-range distance restraints (in the range of 10–60 Å) as well as relative orientations on the basis of the anisotropy of the magnetic susceptibility of paramagnetic metals.[61] PCSs offer opportunities to determine structures of proteins and protein-protein complexes. The PCS results from the dipolar coupling between the time averaged magnetic moment of the unpaired electron(s) of lanthanoid ion (Ln^{3+}) and that of a given nucleus. Figure 11 illustrates the $\Delta\chi$ tensor of Ln^{3+}-CLaNP-7 on a given protein surface.

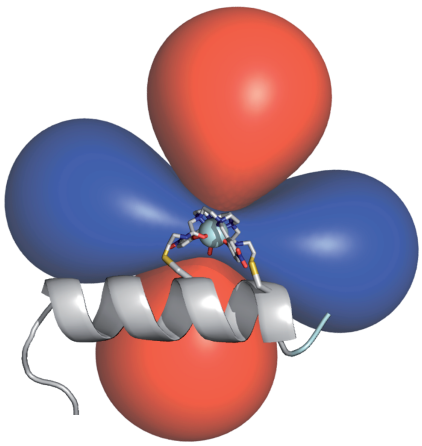

Figure 11. Cartoon representation of anisotropy of magnetic susceptibility of Yb^{3+}-CLaNP-7. Sticks and ribbon show a model of CLaNP-7 on α-helix of a protein. Blue and red isosurfaces represent a nucleus with a PCS of a –1 and +1 ppm, respectively.

PCS can be described by the following equation:

$$\mathrm{PCS} = \frac{1}{12\pi r^3}\left[\Delta\chi_{\mathrm{ax}}\left(3\cos^2\theta - 1\right) + \frac{3}{2}\Delta\chi_{\mathrm{rh}}\left(\sin^2\theta\cos 2\Omega\right)\right]$$

where θ and Ω are angles of position vectors of a given nucleus with respect to the reference frame of magnetic susceptibility tensor. *r* represents the distance between the unpaired electron of Ln^{3+} and a given nucleus (Figure 12).[61] The magnitude of the PCS is proportional to the inverse third power of the distance, which allows for obtaining long-range distance information compared to relaxation, which scales with r^6. The anisotropy of magnetic susceptibility is described by axial ($\Delta\chi_{ax}$) and rhombic ($\Delta\chi_{rh}$) components.

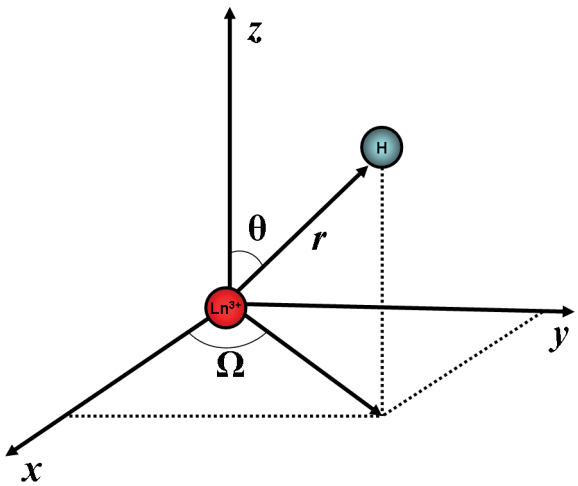

Figure 12. Coordinate system describing PCS. Red and blue spheres represent a paramagnetic metal and an observed nucleus, respectively.

Residual dipolar coupling

Residual dipolar couplings (RDCs) were initially recognized as a useful NMR tool to provide distance independent orientation restraints for structure refinement. Nowadays, the application of RDC has been expanded to structure determination of protein-protein complexes.[61] RDC also offers valuable information about dynamics in proteins and protein-protein interactions.[62]

The RDC can be detected when tumbling of proteins is not completely isotropic but partially aligned with the external magnetic field. This is often achieved by addition of external alignment media to protein samples. Alternatively, paramagnetic metals, either natural present[63] or artificially introduced, to the protein of interest.[61] Partial

alignment of biomolecules leads to incomplete averaging of dipole-dipole interaction between two spins. The resulting residual dipolar couplings provide information about the orientation of the protein relative to the external magnetic field.[61]

Paramagnetic relaxation enhancement

Paramagnetic relaxation enhancement (PRE) was originally considered to be deleterious or at least a nuisance effect when metalloenzymes were investigated by NMR spectroscopy. Essential information about the active site was lost due to the fact that resonances of nuclei close to the metal were broadened out beyond detection. PRE arises from the dipole-dipole interactions of an unpaired electron in the paramagnetic center with nuclei in the proximity. PRE effect is dependent on the inverse sixth power of distance between an unpaired electron and a given nucleus.[44, 64] In comparison with the NOE effect, which yields measureable distances up to 6 Å, PRE causes effects over distances up to 20 Å and in some cases even up to 45 Å.[60, 64] The deleterious effect of line broadening by PRE was soon turned into a useful tool for NMR experiments. By artificially introducing an unpaired electron in a paramagnetic center into protein samples, PRE can be used as a molecular ruler, due to the strong distance dependency.[44] PRE is also extremely sensitive to lowly populated states of protein conformations and protein complexes.[64-67] Nowadays, PRE is the most common paramagnetic NMR experiment to determine distance restraints for structure determination of proteins and transient protein-protein complexes.[44, 61]

Thesis outline

At the start of this research in 2009, a model of Pdx-P450cam complex was available.[68] This model was generated on the basis of a series of NMR data and showed good correlations with earlier mutagenesis results. To test the validity of this model and further characterize the dynamics of Pdx-P450cam interaction, we decided to carry out paramagnetic NMR analysis. In Chapter 2, the attachment of a paramagnetic NMR probe, CLaNP-7, is evaluated at multiple sites of Pdx and P450cam. The $\Delta\chi$ tensors of Ln^{3+}-CLaNP-7 were experimentally determined by PCS analysis. These results form the prelude for the intermolecular paramagnetic NMR experiments to study the Pdx-P450cam complex discussed in Chapter 3. To calculate the structure of the Pdx-P450cam complex, 446 inter-protein distance and orientation restraints were used on the basis of the PCS, RDC and PRE experiments. After the structure had been determined by paramagnetic NMR analysis, our collaborator, Dr. Nojiri and co-workers in Osaka University (Japan) solved the crystal structure of the complex at a resolution of 2.5 Å. The crystal structure is identical to the solution structure within the variation of the ensemble. Compared with the previous model, the orientation of Pdx is rotated by 90° perpendicular to the axis of P450cam heme. The structural analysis of the binding interface revealed potential ET transfer pathways and important interactions between

Pdx Asp38 and P450cam Arg112 as well as hydrophobic contacts between Trp106 and P450cam Ala113. Moreover, several polar residues are found in the interface that had not been recognized to be relevant for binding before. In Chapter 4, site-directed mutagenesis and kinetic measurements were employed to probe the energetic importance and role of the polar residues in the Pdx-P450cam interaction. The results of the paramagnetic NMR analysis used for the structure calculations of the complex suggested the presence of an encounter sate in the Pdx-P450cam complex. To characterize this lowly populated state, Gd^{3+} loaded CLaNP-7 as well as an MTSL spin labels were attached at six different positions on Pdx and P450cam surfaces and inter-protein PRE analysis was performed (Chapter 5). Dynamics in the P450cam enzyme is observed not only for the protein-protein interaction but also for the substrate binding process. Most of the crystal structures of P450cam exhibit a closed conformation in which there is no channel large enough for substrate to access the active site. In Chapter 6, using paramagnetic substrate analogues, the substrate access channel of P450cam was investigated by X-ray crystallography and paramagnetic NMR analysis. Finally, in the concluding remarks, the results from these chapters are discussed in relation to recent studies of the effector role of Pdx in the P450cam catalytic system.

References

1. T. Omura *Proc Jpn Acad Ser B Phys Biol Sci*. **2011**, *87*, 617-640.
2. R. W. Estabrook, D. Y. Cooper, O. Rosenthal *Biochem Z*. **1963**, *338*, 741-755.
3. D. Y. Cooper, S. Levin, S. Narasimhulu, O. Rosenthal *Science*. **1965**, *147*, 400-402.
4. T. Sakaki *Biol Pharm Bull*. **2012**, *35*, 844-849.
5. D. R. Nelson, D. C. Zeldin, S. M. Hoffman, L. J. Maltais, H. M. Wain, D. W. Nebert *Pharmacogenetics*. **2004**, *14*, 1-18.
6. D. W. Nebert, M. Adesnik, M. J. Coon, R. W. Estabrook, F. J. Gonzalez, F. P. Guengerich, I. C. Gunsalus, E. F. Johnson, B. Kemper, W. Levin, et al. *DNA*. **1987**, *6*, 1-11.
7. D. H. Peterson, H. C. Murray *J Am Chem Soc*. **1952**, *74*, 1871-1872.
8. S. B. Mahato, S. Garai *Steroids*. **1997**, *62*, 332-345.
9. Y. Katsumoto, M. Fukuchi-Mizutani, Y. Fukui, F. Brugliera, T. A. Holton, M. Karan, N. Nakamura, K. Yonekura-Sakakibara, J. Togami, A. Pigeaire, G. Q. Tao, N. S. Nehra, C. Y. Lu, B. K. Dyson, S. Tsuda, T. Ashikari, T. Kusumi, J. G. Mason, Y. Tanaka *Plant Cell Physiol*. **2007**, *48*, 1589-1600.
10. M. Katagiri, B. N. Ganguli, I. C. Gunsalus *J Biol Chem*. **1968**, *243*, 3543-3546.
11. T. L. Poulos, B. C. Finzel, I. C. Gunsalus, G. C. Wagner, J. Kraut *J Biol Chem*. **1985**, *260*, 16122-16130.
12. O. Pylypenko, I. Schlichting *Annu Rev Biochem*. **2004**, *73*, 991-1018.
13. Y. T. Lee, R. F. Wilson, I. Rupniewski, D. B. Goodin *Biochemistry*. **2010**, *49*, 3412-3419.
14. S. G. Sligar, I. C. Gunsalus *Proc Natl Acad Sci U S A*. **1976**, *73*, 1078-1082.
15. V. Y. Kuznetsov, T. L. Poulos, I. F. Sevrioukova *Biochemistry*. **2006**, *45*, 11934-11944.
16. I. F. Sevrioukova, T. L. Poulos *Arch Biochem Biophys*. **2011**, *507*, 66-74.
17. I. Schlichting, J. Berendzen, K. Chu, A. M. Stock, S. A. Maves, D. E. Benson, R. M. Sweet, D. Ringe, G. A. Petsko, S. G. Sligar *Science*. **2000**, *287*, 1615-1622.
18. A. R. Dunn, I. J. Dmochowski, A. M. Bilwes, H. B. Gray, B. R. Crane *Proc Natl Acad Sci U S A*. **2001**, *98*, 12420-12425.
19. T. L. Poulos *Biochem Bioph Res Co*. **2003**, *312*, 35-39.

20. B. OuYang, S. S. Pochapsky, G. M. Pagani, T. C. Pochapsky *Biochemistry*. **2006**, *45*, 14379-14388.
21. W. K. Myers, Y. T. Lee, R. D. Britt, D. B. Goodin *J Am Chem Soc*. **2013**, *135*, 11732-11735.
22. S. Nagano, T. L. Poulos *J Biol Chem*. **2005**, *280*, 31659-31663.
23. E. K. Asciutto, M. Dang, S. S. Pochapsky, J. D. Madura, T. C. Pochapsky *Biochemistry*. **2011**, *50*, 1664-1671.
24. E. K. Asciutto, M. J. Young, J. Madura, S. S. Pochapsky, T. C. Pochapsky *Biochemistry*. **2012**, *51*, 3383-3393.
25. I. F. Sevrioukova, T. L. Poulos *J Biol Chem*. **2012**, *287*, 3510-3517.
26. I. F. Sevrioukova *J Mol Biol*. **2005**, *347*, 607-621.
27. T. C. Pochapsky, M. Kuti, S. Kazanis *J Biomol NMR*. **1998**, *12*, 407-415.
28. I. F. Sevrioukova, C. Garcia, H. Li, B. Bhaskar, T. L. Poulos *J Mol Biol*. **2003**, *333*, 377-392.
29. N. Sari, M. J. Holden, M. P. Mayhew, V. L. Vilker, B. Coxon *Biochemistry*. **1999**, *38*, 9862-9871.
30. S. G. Sligar, P. G. Debrunner, J. D. Lipscomb, M. J. Namtvedt, I. C. Gunsalus *Proc Natl Acad Sci U S A*. **1974**, *71*, 3906-3910.
31. E. K. Asciutto, J. D. Madura, S. S. Pochapsky, B. OuYang, T. C. Pochapsky *J Mol Biol*. **2009**, *388*, 801-814.
32. B. OuYang, S. S. Pochapsky, M. Dang, T. C. Pochapsky *Structure*. **2008**, *16*, 916-923.
33. L. Rui, S. S. Pochapsky, T. C. Pochapsky *Biochemistry*. **2006**, *45*, 3887-3897.
34. S. Tripathi, H. Li, T. L. Poulos *Science*. **2013**, *340*, 1227-1230.
35. M. Unno, J. F. Christian, D. E. Benson, N. C. Gerber, S. G. Sligar, P. M. Champion *J Am Chem Soc*. **1997**, *119*, 6614-6620.
36. I. F. Sevrioukova, H. Li, T. L. Poulos *J Mol Biol*. **2004**, *336*, 889-902.
37. J. J. Muller, A. Lapko, G. Bourenkov, K. Ruckpaul, U. Heinemann *J Biol Chem*. **2001**, *276*, 2786-2789.
38. J. Schilder, M. Ubbink *Curr Opin Struct Biol*. **2013**, *23*, 911-918.
39. Z. X. Liang, I. V. Kurnikov, J. M. Nocek, A. G. Mauk, D. N. Beratan, B. M. Hoffman *J Am Chem Soc*. **2004**, *126*, 2785-2798.
40. Z. X. Liang, J. M. Nocek, K. Huang, R. T. Hayes, I. V. Kurnikov, D. N. Beratan, B. M. Hoffman *J Am Chem Soc*. **2002**, *124*, 6849-6859.
41. Q. Bashir, A. N. Volkov, G. M. Ullmann, M. Ubbink *J Am Chem Soc*. **2010**, *132*, 241-247.
42. Y. C. Kim, C. Tang, G. M. Clore, G. Hummer *Proc Natl Acad Sci U S A*. **2008**, *105*, 12855-12860.
43. S. Scanu, J. M. Foerster, G. M. Ullmann, M. Ubbink *J Am Chem Soc*. **2013**, *135*, 7681-7692.
44. M. Ubbink *Febs Lett*. **2009**, *583*, 1060-1066.
45. X. Xu, W. Reinle, F. Hannemann, P. V. Konarev, D. I. Svergun, R. Bernhardt, M. Ubbink *J Am Chem Soc*. **2008**, *130*, 6395-6403.
46. Z. X. Liang, M. Jiang, Q. Ning, B. M. Hoffman *J Biol Inorg Chem*. **2002**, *7*, 580-588.
47. K. E. Wheeler, J. M. Nocek, D. A. Cull, L. A. Yatsunyk, A. C. Rosenzweig, B. M. Hoffman *J Am Chem Soc*. **2007**, *129*, 3906-3917.
48. B. M. Hoffman, L. M. Celis, D. A. Cull, A. D. Patel, J. L. Seifert, K. E. Wheeler, J. Wang, J. Yao, I. V. Kurnikov, J. M. Nocek *Proc Natl Acad Sci U S A*. **2005**, *102*, 3564-3569.
49. L. B. Banci, I.; Eltis, L. D.; Felli, I. C.; Kastrau, D. H.; Luchinat, C.; Piccioli, M.; Pierattelli, R.; Smith, M. *Eur J Biochem*. **1994**, *225*, 715-725.
50. I. D. Bertini, A.; Jimenez, B.; Luchinat, C.; Parigi, G.; Piccioli, M.; Poggi, L. *J Biomol NMR*. **2001**, *21*, 85-98.
51. I. L. Bertini, C.; Parigi, G. *Elsevier, Amsterdam*. **2001**.
52. I. Bertini, M. B. Janik, Y. M. Lee, C. Luchinat, A. Rosato *J Am Chem Soc*. **2001**, *123*, 4181-4188.
53. R. Barbieri, I. Bertini, G. Cavallaro, Y. M. Lee, C. Luchinat, A. Rosato *J Am Chem Soc*. **2002**, *124*, 5581-5587.
54. X. C. Su, K. McAndrew, T. Huber, G. Otting *J Am Chem Soc*. **2008**, *130*, 1681-1687.
55. L. J. Martin, M. J. Hahnke, M. Nitz, J. Wohnert, N. R. Silvaggi, K. N. Allen, H.

Schwalbe, B. Imperiali *J Am Chem Soc*. **2007**, *129*, 7106-7113.

56. C. O. Ma, S. J. *J Magn Reson*. **2000**, *146*, 381-384.
57. X. C. Su, T. Huber, N. E. Dixon, G. Otting *Chembiochem*. **2006**, *7*, 1599-1604.
58. W. M. Liu, P. H. Keizers, M. A. Hass, A. Blok, M. Timmer, A. J. Sarris, M. Overhand, M. Ubbink *J Am Chem Soc*. **2012**, *134*, 17306-17313.
59. M. Prudencio, J. Rohovec, J. A. Peters, E. Tocheva, M. J. Boulanger, M. E. Murphy, H. J. Hupkes, W. Kosters, A. Impagliazzo, M. Ubbink *Chem Eur J*. **2004**, *10*, 3252-3260.
60. Y. Hiruma, M. A. Hass, Y. Kikui, W. M. Liu, B. Olmez, S. P. Skinner, A. Blok, A. Kloosterman, H. Koteishi, F. Lohr, H. Schwalbe, M. Nojiri, M. Ubbink *J Mol Biol*. **2013**, *425*, 4353-4365.
61. P. H. Keizers, M. Ubbink *Prog Nucl Magn Reson Spectrosc*. **2011**, *58*, 88-96.
62. J. R. Tolman, K. Ruan *Chem Rev*. **2006**, *106*, 1720-1736.
63. J. R. Tolman, J. M. Flanagan, M. A. Kennedy, J. H. Prestegard *Proc Natl Acad Sci U S A*. **1995**, *92*, 9279-9283.
64. Q. Bashir, S. Scanu, M. Ubbink *Febs J*. **2011**, *278*, 1391-1400.
65. G. M. Clore, J. Iwahara *Chem Rev*. **2009**, *109*, 4108-4139.
66. C. Tang, J. Iwahara, G. M. Clore *Nature*. **2006**, *444*, 383-386.
67. J. Y. Suh, C. Tang, G. M. Clore *J Am Chem Soc*. **2007**, *129*, 12954-12955.
68. W. Zhang, S. S. Pochapsky, T. C. Pochapsky, N. U. Jain *J Mol Biol*. **2008**, *384*, 349-363.